

# Overview of SIMS-Based Experimental Studies of Tracer Diffusion in Solids and Application to Mg Self-Diffusion

Nagraj S. Kulkarni, Robert J. Bruce Warmack, Bala Radhakrishnan, Jerry L. Hunter, Yongho Sohn, Kevin R. Coffey, Graeme E. Murch, and Irina V. Belova

(Submitted August 5, 2014; in revised form August 28, 2014; published online September 23, 2014)

Tracer diffusivities provide the most fundamental information on diffusion in materials, and are the foundation of robust diffusion databases that enable the use of the Onsager phenomenological formalism with no major assumptions. Compared to traditional radiotracer techniques that utilize radioactive isotopes, the secondary ion mass spectrometry (SIMS)-based thin-film technique for tracer diffusion is based on the use of enriched stable isotopes that can be accurately profiled using SIMS. An overview of the thin-film method for tracer diffusion studies using stable isotopes is provided. Experimental procedures and techniques for the measurement of tracer diffusion coefficients are presented for pure magnesium, which presents some unique challenges due to the ease of oxidation. The development of a modified Shewmon-Rhines diffusion capsule for annealing Mg and an ultra-high vacuum system for sputter deposition of Mg isotopes are discussed. Optimized conditions for accurate SIMS depth profiling in polycrystalline Mg are provided. An automated procedure for correction of heat-up and cool-down times during tracer diffusion annealing is discussed. The non-linear fitting of a SIMS depth profile data using the thin-film Gaussian solution to obtain the tracer diffusivity along with the background tracer concentration and tracer film thickness is demonstrated. An Arrhenius fit of the Mg self-diffusion data obtained using the low-temperature SIMS measurements from this study and the high-temperature radiotracer measurements of Shewmon and Rhines (Trans. AIME 250:1021–1025, 1954) was found to be a good representation of both types of diffusion data over a broad range of temperatures between 250 and 627 °C (523 and 900 K).

**Keywords** database, diffusion, isotope, magnesium, self diffusivity, SIMS, tracer diffusivity

This article is an invited paper selected from presentations at the Hume-Rothery Award Symposium on “Thermodynamics and Kinetics of Engineering Materials,” during TMS 2014, held February 16–20, 2014, in San Diego, CA, and has been expanded from the original presentation. This symposium was held in honor of the 2014 Hume-Rothery award recipient, Rainer Schmid-Fetzer, for his seminal contributions to alloy thermodynamics and phase diagrams, both computationally and experimentally.

Electronic supplementary material The online version of this article (doi:10.1007/s11669-014-0344-4) contains supplementary material, which is available to authorized users.

**Nagraj S. Kulkarni**, Knoxville, TN, USA; **Robert J. Bruce Warmack**, and **Bala Radhakrishnan**, Oak Ridge National Laboratory, Oak Ridge, TN, USA; **Jerry L. Hunter**, Virginia Polytechnic Institute and State University, Blacksburg, VA, USA; **Yongho Sohn**, and **Kevin R. Coffey**, University of Central Florida, Orlando, FL, USA; and **Graeme E. Murch**, and **Irina V. Belova**, The University of Newcastle, Callaghan, NSW, Australia. Contact e-mail: Nagraj@alumni.ufl.edu.

## 1. Introduction

Diffusion in multicomponent systems has been best described using the Onsager flux equations of irreversible processes that are based on linear relations between the fluxes and driving forces in the lattice frame of reference.<sup>[1,2]</sup> Under isothermal, isobaric conditions these relations are given by

$$J_i = - \sum_{j=1}^n L_{ij} \frac{\partial \mu_j}{\partial x} \quad (i = 1, 2, \dots, n) \quad (\text{Eq 1})$$

where  $J_i$  is the intrinsic flux of component  $i$ , the  $L_{ij}$ 's are the phenomenological coefficients and are governed by Onsager reciprocal relations,  $L_{ij} = L_{ji}$ ;  $\mu_j$  is the chemical potential of component  $j$ ;  $n$  is the number of components in the system; and  $x$  is the position in the diffusion direction, assuming one-dimensional diffusion. In the absence of external driving forces, the driving forces for diffusion are the chemical potential gradients ( $\partial \mu_j / \partial x$ ), which can be obtained from knowledge of the positional dependence of the composition and the relations between the chemical potentials and composition, which are available from the thermodynamic model of the system under consideration. Additional driving forces due to non-equilibrium vacancy concentrations are usually ignored, if an equilibrium concentration of vacancies is maintained during the diffu-

sion process due to the existence of sufficient sources and sinks throughout the diffusion zone. The phenomenological coefficients are unique in that they are independent of the driving force and functions of only the local composition. Since in ordinary diffusion couple experiments, chemical potential gradients are not directly measured, it is very difficult to directly measure the phenomenological coefficients. Hence, relations between the phenomenological coefficients and other measurable kinetic quantities such as tracer, intrinsic and interdiffusion coefficients are utilized since the driving forces in the flux expressions involving those coefficients are given in terms of concentration gradients. Among the various diffusion coefficients, the approximate Manning relations<sup>[3–5]</sup> between the tracer diffusion coefficients and the phenomenological coefficients, originally obtained using a random alloy model, are the most useful since these permit the determination of the complete  $L_{ij}$  matrix. These are

$$L_{ii} = \frac{c_i D_i^*}{k_B T} \left[ 1 + \frac{2c_i D_i^*}{M_0 \sum_k c_k D_k^*} \right] \quad (\text{Eq 2})$$

$$L_{ij} = \frac{2c_i D_i^* c_j D_j^*}{k_B T (M_0 \sum_k c_k D_k^*)} \quad \text{for } i \neq j \quad (\text{Eq 3})$$

where  $k_B$  is the Boltzmann constant,  $c_i$  is the concentration ( $\text{at.}/m^3$ ) and  $D_i^*$  is the tracer diffusion coefficient ( $m^2/s$ ) of component  $i$ ,  $T$  is the absolute temperature (K),  $M_0 = 2f_0/(1 - f_0)$ , and  $f_0$  is the geometric correlation factor that is defined by the relevant crystal structure, e.g., it is 0.78146 for the face-centered cubic (fcc) lattice. For the hexagonal-close-packed (hcp) Mg lattice, the diffusion anisotropy estimated by Allnatt et al.,<sup>[6]</sup> when averaged over the polycrystalline environment, and making use of the calculations by Koiwa and Ishioka,<sup>[7]</sup> gives an averaged  $f_0$  of about 0.783, which is very close to the value of  $f_0$  in the fcc lattice. More exact relations between the phenomenological and tracer diffusion coefficients are obtained from the Moleko, Allnatt and Allnatt (MAA) formalism<sup>[8]</sup> but these are not available in closed form and have to be solved numerically.

The relations between intrinsic, interdiffusion and phenomenological diffusion coefficients in multicomponent systems are more complex<sup>[9,10]</sup> and are not considered here, but simplifications are possible if the off-diagonal terms in the  $L_{ij}$  matrix can be ignored (i.e., the Darken<sup>[11]</sup> assumption) as shown by Kirkaldy.<sup>[9]</sup> In fact, this is utilized by the diffusion software, DICTRA<sup>[12,13]</sup> for creating mobility diffusion databases based on the diagonal ( $L_{ii}$ ) terms in the  $L_{ij}$  matrix, where the mobility  $M_i$  is related to  $L_{ii}$  by

$$L_{ii} = \frac{c_i D_i^*}{k_B T} = c_i M_i \quad \text{if } L_{ij} = 0 \quad (\text{Eq 4})$$

The above Darken assumption implies that correlation and vacancy-wind factors in diffusion are neglected although this may not always be justified.<sup>[3,4]</sup> It should be pointed out that it is not possible solely from interdiffusion coefficients obtained from diffusion couple experiments carried out in the laboratory frame of reference, to obtain the

complete  $L_{ij}$  matrix, since these ( $L_{ij}$ ) are defined in the lattice frame of reference and have additional degrees of freedom. The determination of intrinsic diffusion coefficients that are defined in the lattice reference frame involves difficult experiments that require inert lattice marker displacement measurements.<sup>[2,14,15]</sup> Hence, data on intrinsic diffusivities are very difficult to obtain. Additionally, interdiffusion and intrinsic diffusion experiments in higher order (three or more) multicomponent systems are extremely difficult to carry out due to the difficulty in designing suitable diffusion couples with intersecting diffusion composition paths.<sup>[9]</sup> Thus from a practical viewpoint, adequate tracer diffusion data is always necessary to construct a suitable mobility diffusion database that is based on an optimized assessment of various types of diffusion data.<sup>[13,16]</sup> A diffusion database entirely based on tracer diffusion coefficients alone, besides being easier to comprehend physically, can conveniently provide the complete matrix of phenomenological coefficients with the use of the Manning (Eq 2, 3)<sup>[4]</sup> or MAA<sup>[8]</sup> relations. Thus if the objective is to provide a rigorous description of multicomponent diffusion for materials design initiatives such as Integrated Computational Materials Engineering (ICME)<sup>[17]</sup> and the Materials Genome Initiative (MGI),<sup>[18]</sup> the use of the complete Onsager formalism (Eq 1) and the associated tracer diffusion database is recommended. Additionally, extension of a bulk tracer diffusion database to include anisotropy in diffusivities,<sup>[19,20]</sup> grain boundary and interfacial diffusivities<sup>[21]</sup> is conveniently done using diffusion data obtained from single crystal, grain boundary and surface tracer diffusion measurements respectively.

Historically, tracer diffusion data have been obtained using the thin-film technique with radioactive isotopes serving as tracers.<sup>[22–24]</sup> Due to the safety and cost issues associated with radioactive tracer diffusion measurements, except for a few select locations (e.g., University of Münster), such measurements have become scarce. Radio-tracer diffusion studies carried out at federal laboratories in the United States, such as Argonne National Laboratory, have significantly diminished since the 1970s. An alternative tracer diffusion technique that utilizes enriched stable isotopes rather than radioactive isotopes as tracers is based on the use of secondary ion mass spectrometry (SIMS).<sup>[25,26]</sup> In the SIMS technique, a primary ion beam ( $\text{Cs}^+$ ,  $\text{O}_2^+$ ,  $\text{O}^-$ , etc.) is used to sputter off the surface layers (few nm) of a solid sample, partially as secondary ions, that are then collected and analyzed for concentrations (intensities) using a mass spectrometer. Modern SIMS instruments (e.g., from Cameca) permit continuous analysis of isotopes in the secondary ion beam during the sputter process. With knowledge of the sputter rate, the depth of the sputtered crater in a sample at any time can be directly correlated with the instantaneous isotopic concentration that is linearly related to secondary ion intensity corresponding to that isotope, thus permitting depth profile measurements to be carried out. The main benefit of SIMS is that it can distinguish between various isotopes of the same element, e.g., <sup>24, 25, 26</sup>Mg (mass resolution up to 20,000.1  $\text{mamu}/\Delta m$ ), using a highly discriminating mass spectrometric technique, e.g., magnetic sector SIMS,<sup>[27,28]</sup> and also measure extre-

mely small concentrations (ppm to ppb levels) of the isotope as a function of depth, which is an essential requirement for tracer diffusion measurements in order to be in the dilute limit. SIMS has a very good depth resolution of few nm, and a lateral resolution (scanned area) that is typically in the tens of  $\mu\text{m}$  for the desired detection level in SIMS instruments that are suitable for tracer diffusion measurements, e.g., Cameca IMS 3f-7f series. The capability of three-dimensional composition mapping of very dilute levels of impurities or isotopes is another special feature of the SIMS technique.

Because of the small probe size, SIMS can directly carry out tracer diffusion measurements within single crystal grains of large grained (few hundred  $\mu\text{m}$ ) polycrystalline alloy samples with orientations obtained using the electron backscatter diffraction (EBSD) technique.<sup>[29]</sup> In comparison, similar radiotracer diffusion measurements require the use of specially manufactured large alloy single crystals with dimensions of 5-10 mm (0.005-0.010 m) or greater. Usually, SIMS tracer diffusion measurements are confined to samples subjected to annealing temperatures that are lower than about  $0.6T_M$ , where  $T_M$  is the melting temperature, since the diffusion depths typically measured with SIMS are less than about 15  $\mu\text{m}$ . In some cases, SIMS measurements on samples annealed at higher temperatures ( $0.8T_M$ ) can be carried out using very short annealing times (e.g., 10 min at 475 °C for pure Mg in this study) in order to keep the diffusion depths to within 20  $\mu\text{m}$ . However, for typical annealing times (30 min to a few h) utilized in SIMS-based tracer diffusion experiments, annealing at higher temperatures results in deeper tracer penetration depths (e.g., 20-100  $\mu\text{m}$ ). Such deep profiles can still be measured using discrete SIMS measurements on angled or normally sectioned samples<sup>[30]</sup> in a manner similar to the electron microprobe analysis (EPMA)<sup>[31]</sup> technique. In contrast, radiotracer measurements are usually limited to samples annealed at higher temperatures ( $>0.6T_M$ ) due to the sampling volume requirements for accurate radiation intensity measurements that require much larger tracer penetration depths (few mm or more).

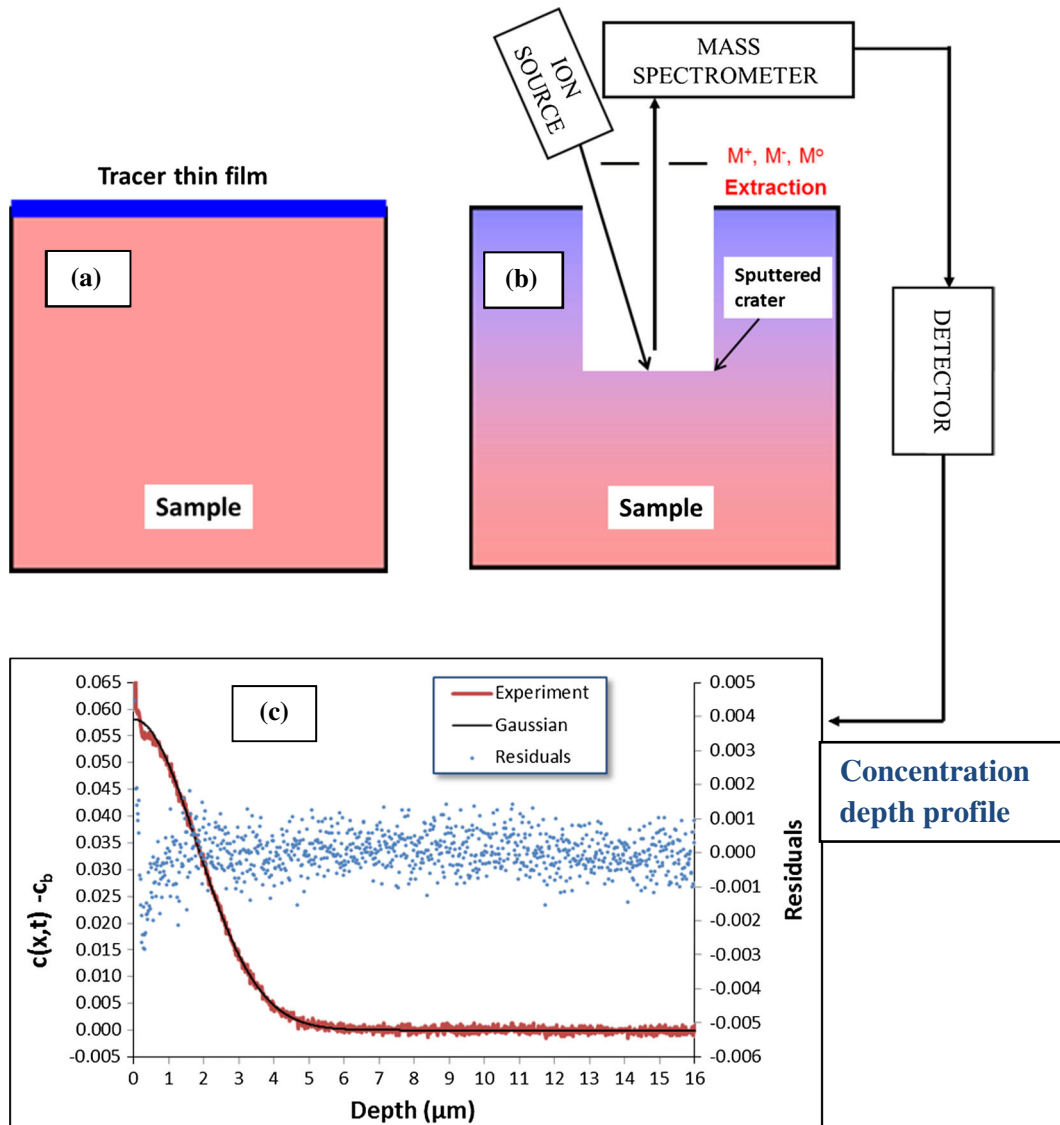
In order to get the tracer diffusivity with the SIMS technique in a polycrystalline material, a suitable average of several measurements within randomly oriented individual grains can be taken. Such measurements are typically within the initial part of the type B regime of diffusion as defined by Harrison.<sup>[26,32,33]</sup> If an effective diffusivity that includes both bulk and grain boundary diffusion contributions is desired (regime A), a smaller grain size sample, e.g., a nanocrystalline sample, is necessary for using the SIMS technique. In comparison, the radiotracer technique directly provides the effective polycrystalline diffusivity in large grained (tens of microns) samples on account of the large sampling volume.<sup>[22,33]</sup>

It is very difficult currently to use the conventional SIMS technique to obtain grain boundary diffusivities using the Harrison regime C because of detection limits, though some applications of Nano-SIMS have recently emerged.<sup>[34]</sup> However, averaged grain boundary impurity diffusivities can be obtained using the second (tail) part of the Harrison B regime.<sup>[26,35]</sup> In comparison, radiotracer measurements are well

suited to measure grain boundary diffusivities both in the B and C kinetic regimes.<sup>[21,33]</sup> The Atom Probe technique,<sup>[36]</sup> which is essentially a mass spectrometric technique with atomic scale resolution, is ideal for specific grain boundary diffusivity measurements in regime C. In this work, only bulk tracer diffusion measurements (within the initial portion of regime B) using the SIMS technique in polycrystalline specimens having large grain sizes (hundreds of  $\mu\text{m}$ ) are considered.

SIMS has been widely used for impurity (dopant) and self-diffusion measurements in electronic, geologic and oxide materials.<sup>[26-28]</sup> A good example of the use of SIMS in single crystal NiAl alloys is discussed by Frank et al.,<sup>[37]</sup> who used the SIMS technique in order to extend their high temperature ( $>\sim 1200$  K) tracer diffusion measurements to lower temperatures ( $<1200$  K). SIMS-based tracer diffusion studies in polycrystalline metals and alloy systems, such as those in magnesium (Mg) considered in this work, pose special problems in experimentation due to the ease of oxidation. The polycrystalline nature of metals also presents challenges with the SIMS depth profiling technique due to measurement errors introduced caused by sputter-induced roughening. Furthermore, the accuracy needed for SIMS tracer diffusion measurements is only available with sophisticated instruments, such as those from Cameca, and are not widely available due to the high cost. On account of these reasons, SIMS-based tracer diffusion measurements in polycrystalline metals and alloys are relatively rare. The present work represents the first attempt in developing the SIMS-based tracer diffusion technique for polycrystalline Mg.

The automotive industry is considering the use of Mg alloys as a replacement for steel and aluminium alloy components on account of its better strength to weight ratio.<sup>[38]</sup> For the purpose of accelerated design of suitable Mg alloy components, the ICME of Mg requires the availability of Mg diffusion databases for which tracer diffusion data in Mg and its alloys is necessary. Most of the available tracer diffusion data in the Mg alloy system is self-diffusion data, i.e., diffusion of Mg in pure Mg, and includes both single and polycrystalline data. There are considerable data on impurity diffusion of various elements in pure Mg<sup>[39]</sup> that have been obtained using both the radiotracer<sup>[40,41]</sup> and SIMS techniques,<sup>[42]</sup> as well as first-principles methods.<sup>[43]</sup> The available Mg self-diffusion data have been obtained using the radiotracer technique, which has provided Mg tracer diffusion data at high temperatures ( $>450$ - $650$  °C) in polycrystals<sup>[44]</sup> and single crystals.<sup>[19,45]</sup> Since many processing treatments (e.g., warm rolling, extrusion, precipitation annealing, etc.) as well as service conditions of Mg alloys involve the use of much lower temperatures, it is essential to have a diffusion database that covers a broad range of temperatures. The present study provides some low and intermediate temperature tracer diffusion data for pure Mg. Experimental techniques for Mg isotopic thin-film sputter deposition and diffusion annealing with minimal oxidation, accurate temperature control, and optimization of SIMS parameters for reliable depth profiling of Mg isotopes are provided. Analytical procedures for analysis of SIMS data, including corrections for heat-up and cool-down times during tracer diffusion experiments are also discussed.



$$c(x, t) - c_b = (c_0 - c_b) \frac{h}{\sqrt{\pi D^* t}} \exp\left(-\frac{x^2}{4D^* t}\right) \quad \text{if } h \ll 2\sqrt{D^* t}$$

**Thin Film (Gaussian) Solution to extract  $D^*$  using a non-linear fit**

**Fig. 1** SIMS-based stable isotopic technique for tracer diffusion measurements (schematic). From top-left (clockwise): (a) Thin film tracer deposited on sample. (b) After annealing at the desired temperature and time ( $t$ ), SIMS depth profiling is done to obtain the concentration (abundance) as a function of depth. (c) The thin film (Gaussian) solution is used to extract the tracer diffusivity  $D^*$  using a least-squares, non-linear fitting method. The background concentration  $c_b$  and the tracer film thickness,  $h$ , are also obtained with the fitting. The y-coordinate is the excess abundance at any position and the x-coordinate is the position along the diffusion direction

## 2. Thin-Film Technique for Tracer Diffusion

The well-known thin-film method and solution<sup>[22–24]</sup> used in radioactive tracer diffusion measurements is also applicable for such measurements carried out with the SIMS technique where enriched stable isotopes serve as tracers. In

the SIMS approach for tracer diffusion (Fig. 1), initially a film of thickness  $h$  in the form of an enriched stable isotope, e.g.,  $^{25}\text{Mg}$ , is deposited on the surface of a polished sample (e.g., pure Mg or an Mg alloy) that is being investigated. Physical vapor deposition (PVD) techniques such as sputtering or evaporation are the common ones utilized though

other techniques such as electroplating can also be used. The thickness ( $h$ ) of the isotopic tracer film can typically vary from a few nm to hundreds of nm, depending upon the diffusion length,<sup>[24]</sup>  $2\sqrt{D_i^*t}$ , where  $t$  is the diffusion time (s), and  $D_i^*$  is the tracer diffusivity of component  $i$  at the desired temperature,  $T$ , and can be obtained from the activation energy,  $Q_i^*$ , and pre-exponential factor,  $D_{0,i}^*$ , as

$$D_i^* = D_{0,i}^* \exp(-Q_i^*/k_B T) \quad (\text{Eq 5})$$

It should be mentioned that rather than a single enriched isotope that serves as the tracer, the film can contain a mixture of tracers of enriched stable isotopes that correspond to the elements in the alloy in order to permit tracer diffusion measurements of several elements within the same specimen that have been annealed under identical conditions. This is usually avoided since maintaining a given ratio of enriched isotopic concentrations uniformly within the film is difficult due to the challenges in controlling deposition rates over the surface area of the alloy specimen.

The sample containing the deposited tracer film is then carefully annealed at the desired temperature and time under controlled conditions to minimize oxidation and permit diffusion of the tracer in a direction  $x$  that is normal to the surface of the tracer film. The depth profiles of all the isotopes involving the tracer element (e.g.,  $^{24}\text{Mg}$ ,  $^{25}\text{Mg}$  and  $^{26}\text{Mg}$ ) in the sample are then measured using a SIMS instrument capable of accurate depth profiling and isotope discrimination, e.g., magnetic sector or a Time-Of-Flight (TOF) SIMS instruments.<sup>[25-27]</sup> Since depth profiling using the SIMS method can be time intensive ( $\sim 5 \mu\text{m/h}$ ), the tracer diffusion parameters ( $h$ ,  $T$ ,  $t$ ) are initially selected using an estimated or guess value of the activation energy that may be obtained from a variety of sources, including published data or data from similar crystal structures, theoretical<sup>[43]</sup> or empirical<sup>[46]</sup> calculations or interdiffusion experiments,<sup>[2,9]</sup> so that the total diffusion depth ( $6\sqrt{D_i^*t}$ ) probed is less than about  $15 \mu\text{m}$ . Larger penetration depths can still be investigated at the expense of additional SIMS measurement time and the cost associated with thicker tracer films. The choice of the diffusion parameters can be adjusted with an improved estimate of the activation energy based on a few, preliminary tracer diffusion data points at a few temperatures.

## 2.1 Thin-Film Solution

From Fick's first law of diffusion<sup>[1,2,9,24]</sup> the one dimensional tracer diffusion flux,  $J_i$ , is

$$J_i = -D_i^* \frac{\partial c_i}{\partial x} \quad (\text{Eq 6})$$

where  $\partial c_i / \partial x$  is the concentration gradient of the tracer in a direction normal to the surface of the film. Based on the choice of the concentration units ( $\text{at.}/\text{m}^3$  or  $\text{mol}/\text{m}^3$ ), typical units for the flux in the case of solid state diffusion are  $\text{at.}/\text{m}^2\text{s}$  or  $\text{mol}/\text{m}^2\text{s}$ . Fick's second law or the continuity equation in one dimension is

$$\frac{\partial c_i}{\partial t} = -\frac{\partial J_i}{\partial x} = D_i^* \frac{\partial^2 c_i}{\partial x^2} \quad \text{if } D_i^* \text{ is constant} \quad (\text{Eq 7})$$

In the case of an enriched stable isotope used as a tracer, except for an initial transient period at the start of the diffusion anneal, the concentration of the stable isotope in excess of its background concentration in the sample is sufficiently small, and therefore it can be considered to be in the dilute limit. Hence the excess tracer concentration has a negligible effect on the bulk composition of the sample, which means that the tracer diffusivity can be assumed to be constant. In the case of self-diffusion in a pure metal rather than an alloy, the tracer diffusivity is always constant because only the isotopes of the pure metal are present. If radioactive isotopes are used as tracers, the background concentration of the radioactive isotope in the bulk alloy is absent. Again because extremely dilute concentrations of the radioactive tracer are present during the diffusion experiment, the composition of the bulk alloy is unchanged and the tracer diffusivity can be assumed to be constant. In both cases, a test of the constant diffusivity assumption can be made by examining the fit to the solution of the one-dimensional diffusion equation next discussed.

The analysis of the SIMS isotopic depth profile data to obtain the tracer diffusion coefficient is carried out by using the one-dimensional solution to the continuity equation, Eq 7.<sup>[23,24]</sup> The concentration of the selected isotope used as the tracer at any position and time is given by

$$c_i(x, t) - c_{b,i} = \frac{(c_{0,i} - c_{b,i})}{2} \left[ \text{erf} \left( \frac{x+h}{2\sqrt{D_i^*t}} \right) - \text{erf} \left( \frac{x-h}{2\sqrt{D_i^*t}} \right) \right] \quad (\text{Eq 8})$$

where  $c_{0,i}$  is the initial concentration of the tracer  $i$  in the enriched isotopic film at  $t = 0$ , and  $c_{b,i}$  is the naturally occurring or background concentration of the tracer in the sample. The term on the left hand side of Eq 8,  $c_i(x, t) - c_{b,i}$ , is the excess tracer concentration, i.e., the concentration of the tracer over its background concentration.

The initial tracer film is considered to be a thin-film if the film thickness is much smaller than the diffusion length, i.e.,  $h \ll 2\sqrt{D_i^*t}$ . Equation 8 then simplifies to a Gaussian or thin-film solution:

$$c_i(x, t) - c_{b,i} \approx (c_{0,i} - c_{b,i}) \frac{h}{\sqrt{\pi D_i^*t}} \exp \left( -\frac{x^2}{4D_i^*t} \right) \quad (\text{Eq 9})$$

if  $h \ll 2\sqrt{D_i^*t}$

Equation 8 may hence be considered as the thick-film solution that is applicable when the film thickness is not significantly smaller than the diffusion length, e.g., if  $h \leq 2\sqrt{D_i^*t}$ .

Taking the natural log on both sides of Eq 9 gives

$$\begin{aligned} \text{Ln}[c_i(x, t) - c_{b,i}] &= -\frac{x^2}{4D_i^*t} + C_s \quad \text{where } C_s \\ &= \text{Ln} \left[ \frac{h(c_{0,i} - c_{b,i})}{\sqrt{\pi D_i^*t}} \right] \end{aligned} \quad (\text{Eq 10})$$

where  $C_s$  is a constant. In the case of a radioactive tracer, Eq 8 reduces to the well-known thin film solution for

radiotracer diffusion where the background tracer concentration  $c_{b,i}$  is zero.<sup>[20–22]</sup>

$$c_i(x, t) \approx \frac{hc_{0,i}}{\sqrt{\pi D_i^* t}} \exp\left(-\frac{x^2}{4D_i^* t}\right) \quad \text{if } h \ll 2\sqrt{D_i^* t} \text{ and } c_{b,i} = 0 \quad (\text{Eq 11})$$

Taking natural log on both sides of Eq 11 gives

$$\text{Ln}[c_i(x, t)] = -\frac{x^2}{4D_i^* t} + C_r \quad \text{where } C_r = \text{Ln}\left[\frac{hc_{0,i}}{\sqrt{\pi D_i^* t}}\right] \quad (\text{Eq 12})$$

where  $C_r$  is a constant. Eqs 11 and 12 are also applicable to the case of impurity diffusion where the tracer is an impurity element diffusing in the host alloy. The concentration  $c_i(x, t)$  may be replaced by the isotopic abundance (atom fractions) for tracer studies or where the impurity has enriched isotopes since the molar volume is constant. For example, in the present SIMS study, the abundance of  $^{25}\text{Mg}$  is readily measured as a function of depth by measuring the ratio of the  $^{25}\text{Mg}$  intensity to the sum of intensities of all Mg isotopes in the alloy. This procedure also eliminates variations in the incidence ion beam in SIMS. In the case of radioactive tracers, the intensity of the radiation associated with a given position within the sample is directly proportional to the concentration of the tracer.<sup>[22]</sup>

With tracer studies based on radioactive isotopes, the typical concentration range of the tracer that is measurable in the dilute limit varies over several orders of magnitude.<sup>[22,47]</sup> A Gaussian fit, i.e., a linear fit (Eq 12) between the natural log of concentration,  $\text{Ln}[c_i(x, t)]$ , and the square of the penetration distance,  $x^2$ , yields a straight line with slope of  $-1/4D_i^* t$ , which can be conveniently used to extract the tracer diffusivity,  $D_i^*$ , from knowledge of the diffusion time. A similar natural log fit based on Eq 10, if attempted using SIMS tracer data is problematic, since it is adversely affected by the large number of randomly fluctuating data points or noise that can span several orders in magnitude as the tracer concentration approaches the background tracer concentration in the sample (note that  $c_i(x, t) - c_{b,i}$  in Eq 10 can even become negative resulting in imaginary numbers as logarithms are taken). Furthermore, the SIMS dynamic range for accurate tracer concentration beyond the background concentration spans at most one or two orders of magnitude, which can be insufficient for a reliable fit on a log versus  $x^2$  plot. Additionally, it is necessary to know the background tracer concentration,  $c_{b,i}$ , to use Eq 10, unless the tracer is an impurity, in which case Eq 12 can be used (e.g., Al impurity diffusion in Mg<sup>[42]</sup>). The background tracer concentration is usually determined by measuring the tracer concentration deep in the bulk of the sample near the asymptotic limit of the depth profile, where instrument noise becomes more significant. Such deep SIMS measurements also require longer measurement times, and errors due to sputter roughening may increase with increasing depths. Hence, a least square fit of the tracer data<sup>[26]</sup> based on Eq 9 was the method employed in this work (Fig. 1), noting that conditions for the Gaussian thin-film solution ( $h \ll 2\sqrt{D_i^* t}$ ) were always employed. The

initial tracer thickness and the background tracer concentration along with the tracer diffusivity were all simultaneously obtained with the least square fit by including them as fitting parameters. It should be noted that if the conditions for using the thin-film solution are not satisfied, the diffusivities obtained using Eq 8 and 9 will differ, in which case the diffusivity obtained using the thick-film solution (Eq 8) should be the one that is employed.

### 3. Experimental Techniques

SIMS-based tracer diffusion experiments in Mg and its alloys that are readily oxidized and form unstable oxide surface layers pose some unique challenges during various stages of experimentation, including stable isotope target production, thin film deposition, pre-annealing for grain growth and homogenization, Mg-alloy synthesis, sample preparation, tracer diffusion annealing and SIMS measurements. In order to obtain a reliable tracer diffusion measurement, suitable techniques and controls during every stage of experimentation need to be followed. These are highlighted in this discussion.

#### 3.1 Mg Stable Isotopes

Mg consists of three stable isotopes whose natural abundances are:  $^{24}\text{Mg}$ —0.7899,  $^{25}\text{Mg}$ —0.1001,  $^{26}\text{Mg}$ —0.1100. Enriched stable isotopes for all the three isotopes can in principle be used for tracer diffusion studies. Typically, isotopes with lower natural abundance are enriched to higher levels and used as tracers, since a higher enrichment ratio leads to a larger dynamic range for SIMS depth profile measurements. Different techniques are available for isotope enrichment, but isotopes of Mg are primarily enriched using electromagnetic separation devices called calutrons that were originally commissioned at the Oak Ridge National Laboratory (ORNL) during the Manhattan project. The US Department of Energy (DOE) maintains a large repository of stable isotopes separated using calutrons at ORNL. An inventory of stable isotopes for research and other applications can be obtained through the National Isotope Development Center (NIDC<sup>[48]</sup>). Unlike Mg, enriched stable isotopes for many other elements can be manufactured using other production techniques, such as centrifugation, and are available through private companies. For the present study, the minor isotope  $^{25}\text{Mg}$  that was enriched to 0.9787 ( $^{24}\text{Mg}$ —0.0180,  $^{26}\text{Mg}$ —0.0033) was used.

The total cost of the enriched  $^{25}\text{Mg}$  stable isotopic foil used as a target for thin film sputter deposition using a ultra-high vacuum (UHV) system (discussed next) included (1) the unit cost of the enriched stable isotope, (2) the cost of converting the stored oxide form of  $^{25}\text{Mg}$  to a pure  $^{25}\text{Mg}$  metal ingot (which was done by reducing the  $^{25}\text{Mg}$  oxide with gadolinium) and, (3) the subsequent processing cost that involved multiple rolling operations to convert the  $^{25}\text{Mg}$  metal ingot to a foil of the desired dimensions (1 in. or 25.4 mm diameter, 250  $\mu\text{m}$  thick). This processing was carried out at the ORNL isotope processing facility. The

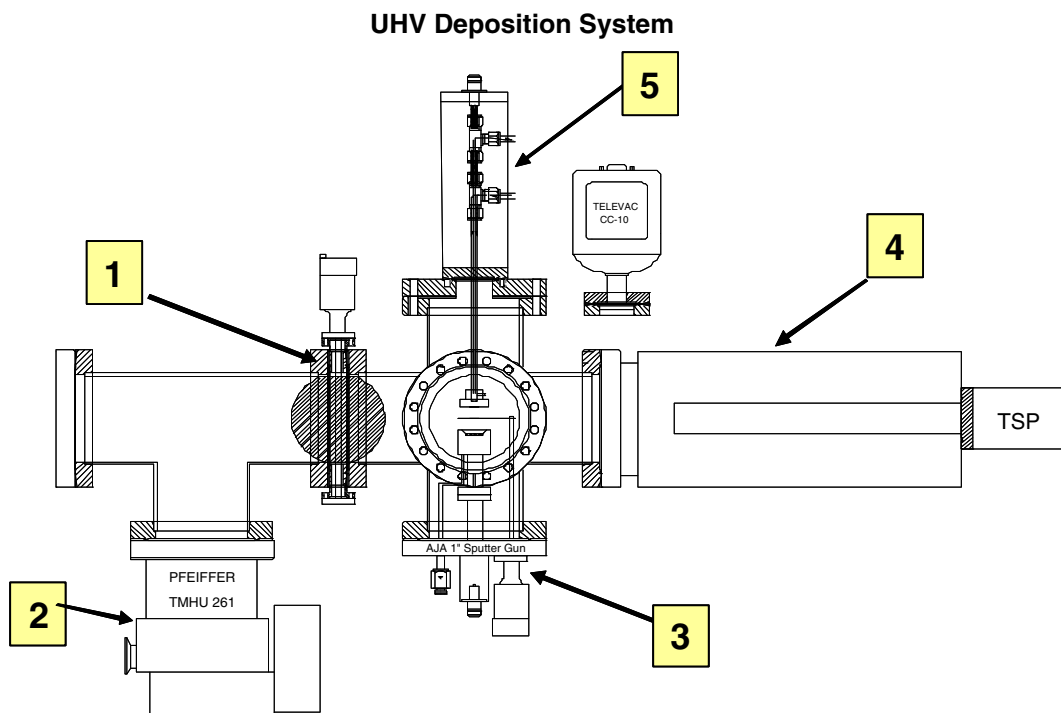
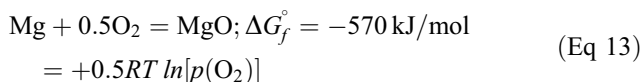


**Fig. 2** UHV deposition system (schematic): 1 = Variable conductance for Ar pressure control; 2 = Turbomolecular pump for Ar; 3 = 1" magnetron sputter deposition with shutter; 4 = Ti sublimation pump for water vapor; 5 = Substrate manipulator with RF power and water cooling (in situ cleaning of sample surface)

diameter of the isotopic  $^{25}\text{Mg}$  foil corresponded to the diameter of the sputter gun in the UHV deposition system in order to facilitate uniform isotope deposition on samples placed within a 1 in. diameter circle on the substrate. The thickness of the foil was selected by taking into consideration the efficiency of sputter deposition (typically  $<5\%$ ), the target utilization efficiency ( $\sim 20\%$  before foil penetration), the desired thickness of the isotopic film ( $\sim 100\text{-}150\text{ nm}$ ), the number of deposition runs, the dimensions and number of samples per run, and finally the total number of samples that could be uniformly coated with the isotopic film before the target isotopic foil was eroded and no longer useable.

### 3.2 UHV System for Mg Thin Film Sputter Deposition

The presence of an initial magnesium oxide ( $\text{MgO}$ ) tracer film on an Mg alloy sample, instead of a pure Mg tracer film, changes the boundary conditions in the thin film solution (Eq 8) used to obtain the tracer diffusivity. It is seen on a Richardson-Ellingham diagram<sup>[49]</sup> for the formation of oxides that the oxidation of Mg is highly favourable energetically compared to most metals in the periodic table:



where  $\Delta G_f^\circ$  is the standard Gibbs free energy of formation of  $\text{MgO}$ . It is essential to have very low levels ( $<10^{-9}$  Torr)

of oxygen (or oxygen sources such as water vapor) during physical vapor deposition (PVD) of Mg in order to prevent oxidation and minimize the oxygen concentration in the deposited Mg films. Conventional PVD systems tend to have vacuum levels that are insufficient ( $\sim 10^{-8}$  Torr) to prevent significant oxygen absorption during Mg deposition. Hence, we designed and constructed an ultra-high vacuum (UHV) magnetron sputter deposition system (Fig. 2) for the deposition of pure Mg films using the  $^{25}\text{Mg}$  isotopic target foil. A background water vapor partial pressure of less than  $10^{-9}$  Torr in the argon (Ar) sputter process gas (99.999% initial purity) used during sputter deposition was obtained with the use of a heated titanium sublimation pump (TSP) that permitted oxygen gettering of the Ar process gas. All metal-sealed-pipes and valves were used for the Ar process gas handling components to prevent re-contamination during transport. Prior to an actual deposition run, it was necessary to pre-bake the UHV chamber for a minimum of a day, while continually pumping the residual water vapor with a high capacity turbo-molecular pump in order to achieve the desired water vapor levels. The substrates (samples) were mounted on water-cooled, magnesium, RF-powered holder that enabled sputter etching of the substrate surface to remove the native oxide film prior to metal film deposition. The Mg stable isotopic foil was bonded on the copper backing plate of the 1 in. AJA International sputter gun using an indium paste.

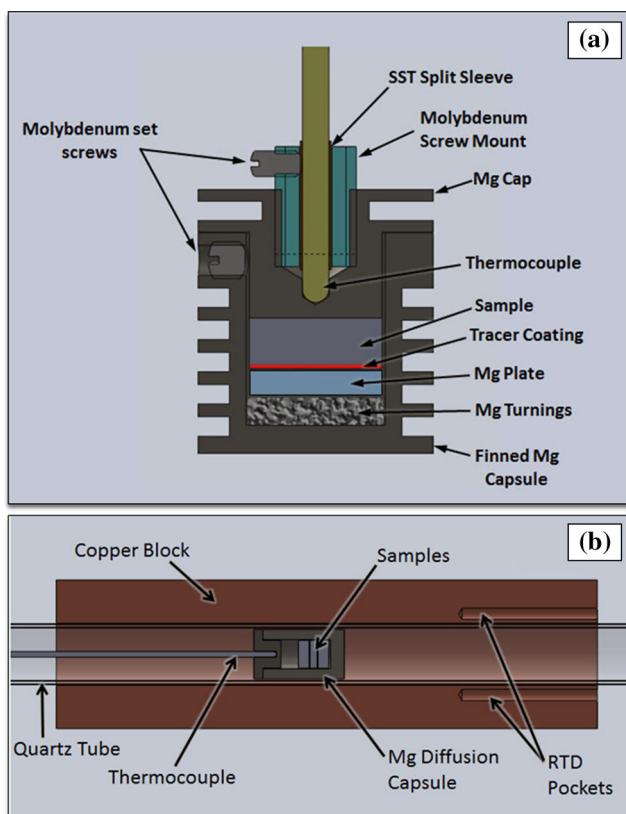


**Fig. 3** Modified Shewmon-Rhines capsule<sup>[44]</sup> and setup: (a) Mg capsule, (b) Setup showing the diffusion capsule inserted in a quartz tube and pushed into the heated copper block region using a thermocouple attached to the cap of the diffusion capsule

### 3.3 Modified Shewmon-Rhines Annealing Capsule

Annealing of magnesium samples placed in inert gas (Ar)-flushed quartz glass tubes results in noticeable oxidation and evaporation loss of the expensive isotope, especially at higher temperatures ( $>300\text{ }^{\circ}\text{C}$ ) where the vapor pressure of Mg becomes noticeable and the kinetics of oxidation increases. To address this, Shewmon and Rhines<sup>[44]</sup> designed a special Mg container with Mg turnings placed in close proximity of the samples to be annealed (Fig. 3a). The Mg capsule was in turn placed in a pyrex glass container and sealed (Fig. 3b). The Mg turnings not only provided the necessary equilibrium vapor pressure over the diffusion samples and prevented evaporative loss, but also protected against oxidation. By placing two active (containing tracer) Mg surfaces facing each other, the loss of the tracer due to evaporation was further minimized. This elegant design was further improved in this work with the use of a permanent quartz tube for containing the Mg capsule vapors (Fig. 3b) in place of the older design<sup>[44]</sup> that used a disposable glass tube. This resulted in higher throughput and lower glass processing costs. The use of a permanent quartz tube also reduced heat-up times of the Mg-capsule containing the Mg samples, since the quartz tube was already at the selected annealing temperature prior to insertion of the Mg capsule by pre-placement in a copper

(Cu) heater block at the desired annealing temperature. The pre-heated Cu heater block had a 17.5 mm pocket for the 17 mm outer diameter quartz enclosure and two 1/8 in. (3.175 mm) RTDs for rapid and accurate equilibration of Mg samples that were placed in the diffusion capsules.

With this new design, the Mg capsule could be quenched in liquid nitrogen, reducing cool-down times. Additionally, a thermocouple (TC) was incorporated in the Mg capsule lid for monitoring the real-time temperature during diffusion annealing experiments, and for corrections on account of heat-up and cool-down times (Fig. 3b). The Mg capsule body was light and small with dimensions: 0.9 in. ( $\sim 23\text{ mm}$ ) length, 0.55 in. ( $\sim 14\text{ mm}$ ) outer diameter (OD), and 0.325 in. ( $\sim 8.3\text{ mm}$ ) inner diameter (ID). It also included fins on the outer walls for more rapid thermal equilibration. The modified capsule was utilized both for pre-annealing Mg samples for grain growth and the tracer diffusion annealing experiments. A number of diffusion capsules were machined for the present work.

For the annealing experiments, an MTI GSL-1100 tube furnace (upper limit  $1200\text{ }^{\circ}\text{C}$ ) with a quartz tube and temperature controller was used. The RTD's were used to calibrate the furnace temperatures and set points for the desired annealing treatments. For accurate temperature control, we calibrated the resistance temperature detectors (Class A RTDs) and TCs (type K) at ORNL's metrology facility using NIST traceable standards. The tolerance for the Class A RTD is  $\pm(0.15 + 0.002 \times T_c)\text{ }^{\circ}\text{C}$ , where  $T_c$  is the temperature in  $^{\circ}\text{C}$ , while that for the TC of type K is  $\pm 2.2\text{ }^{\circ}\text{C}$  between  $-200$  and  $1250\text{ }^{\circ}\text{C}$ .

### 3.4 SIMS Optimization for Mg Depth Profiling

In the present work, SIMS analysis was carried out using a Cameca IMS 7f-Geo system with an  $\text{O}_2^+$  primary ion beam. In comparison to other primary ion beams, the use of an  $\text{O}_2^+$  primary ion beam gives better positive ion yields and improves the depth resolution.<sup>[28]</sup> It should be noted that the  $\text{O}_2^+$  beam does not participate in the tracer diffusion process since the sample is at room temperature in the SIMS system, and the interaction of the  $\text{O}_2^+$  beam with the sample is limited to a few nm at the surface, which is converted to an amorphous oxide and immediately sputtered away for secondary ion signal measurement (SIMS depth profile measurement is continuous). The composition of the Mg isotopes in the annealed sample is unchanged during the SIMS measurement.

The Cameca IMS 7f-Geo system has several important features, including the availability of a range of energy/angle combinations, a continuous primary beam current monitor, a high mass resolution ( $\sim 5,000m/\Delta m$ ) to separate  $25\text{Mg}^+$  from  $(24\text{Mg} + 1\text{H})^+$ , an oxygen (O) leak to increase steady state concentration of oxygen at specimen surface, and dual Faraday cups for high precision stable isotope measurements. For depth profile measurements, a precision of 0.5-1% in the secondary ion signal intensity is typically attainable.

Sputter-induced topography<sup>[28,50]</sup> can be a major source of error in SIMS diffusion depth profile measurements by causing a broadening of the depth profile, thus resulting in a



higher tracer diffusivity. Essentially, it is caused by the interaction of the primary ion beam with the sample volume that causes a variation in the sputter rate along different orientations. This effect is more pronounced in small grained polycrystals (where the average grain size, e.g., a few  $\mu\text{m}$ , is smaller than the primary ion beam spot size, typically  $\sim 10\text{-}50\ \mu\text{m}$ ) having a broad grain size distribution. However, sputter topography is also observed during depth profiling in single crystals or within the interior of large grained polycrystals (grain sizes in hundreds of  $\mu\text{m}$ ). The use of a eucentric rotation stage has been shown to have some success in reducing sputter roughening in polycrystalline matrices,<sup>[51]</sup> however, this capability is not routinely available with most SIMS systems, including the one used in this study, and furthermore, it does not directly address the causes of sputter roughening in single crystals. Additionally, the use of a eucentric rotation stage can introduce complications with the interpretation of signal intensity measurements during depth profiling because of the averaging procedures used.

In certain metallic matrices that readily oxidize (Al, Mg), the sputter topography can be controlled by a suitable optimization of four parameters: (a) the primary ion species ( $\text{O}_2^+$ ,  $\text{Ar}^+$ ,  $\text{Cs}^+$ , etc.), (b) primary ion energy, (c) primary ion bombardment angle, and (d) the oxidative environment that can be affected by the presence of an intentional oxygen (O) leak.<sup>[28]</sup> In order to determine the optimum combination of these parameters, a  $2\ \mu\text{m}$  Mg film was initially sputter-deposited on a single crystal Si wafer. The initial average surface roughness of this film measured using an Atomic Force Microscope (AFM) was about 7 nm. Depth profiling was carried out using a fixed  $\text{O}_2^+$  primary beam over an analysis area of  $\sim 15 \times 15\ \mu\text{m}^2$ . The primary ion angle (measured relative to normal incidence) and energy were varied by changing the primary and secondary accelerating voltages. An oxygen jet was directed at the near surface of the sample to increase the oxygen concentration from a background oxygen backfill condition ( $\sim 1 \times 10^{-9}$  Torr), i.e., no O leak, to an intentional oxygen backfill condition ( $\sim 2 \times 10^{-6}$  Torr). The oxygen partial pressures were measured using the sample chamber ion gauge.

The average AFM roughness at the bottom of the sputtered crater ( $\sim 1\ \mu\text{m}$  depth) for various conditions was measured. In comparison to the typical conditions used during SIMS depth profiling (5 keV primary ion energy,  $45^\circ$  incidence angle, no O leak) that resulted in significant sputter roughening (crater roughness  $\sim 38\ \text{nm}$ ), it was found that the two best conditions that gave the least amount of sputter-induced roughening (crater roughness  $\sim 11\ \text{nm}$  for both conditions) required the presence of an intentional O leak, and required lower impact energies and closer to normal incidence.<sup>[52]</sup> These conditions were: (a) 3 keV,  $37^\circ$ , and (b) 2 keV,  $40.6^\circ$ . The main benefit of the oxygen leak is a higher steady state oxygen concentration that leads to the formation of a thicker and adherent amorphous MgO layer during the depth profiling. Sputtering from such an amorphous oxide layer gives less roughness than that from a weakly oxidized magnesium polycrystalline layer. The combination of a low energy primary ion beam that is closer to normal incidence, and the relatively easy formation

of an amorphous surface oxide layer results in a reduced interaction depth between the primary ion beam and the amorphous/crystalline interface at the bottom of the crater.<sup>[52]</sup> SRIM<sup>[53]</sup> calculations have shown that the interaction depth with the optimal beam conditions is about one half of that under typical conditions that use much larger impact energies at higher primary ion angles with no oxygen leak. By limiting the interaction between the primary ion beam and the amorphous/crystalline interface, the topography caused by formation of ripples at the bottom of the crater is reduced.<sup>[50,52]</sup>

Additional factors that can have a more pronounced impact on sputter roughening during SIMS depth profiling in polycrystalline samples are the grain size and grain size distribution. Initial as-received pure Mg samples obtained in rod forms for the present work showed small grain sizes ( $\sim 10\ \mu\text{m}$ ) with a broad grain size distribution (largest grains at crater bottoms were nearly  $50\ \mu\text{m}$ ) and random orientation (Fig. 4a). Depth profiling measurements ( $^{25/24}\text{Mg}$  intensity ratio as a function of depth) carried out on these as-received samples, using both typical and optimized conditions previously established, showed no discernible difference. The modified Shewmon-Rhines capsule was used to anneal a pure Mg sample ( $\sim 545\ ^\circ\text{C}$ , 14.5 h). This resulted in an increase in the average grain size ( $> 500\ \mu\text{m}$ ), and an orientation that was modified from a random to a more preferred one (Fig. 4b). Depth profiling measurements on the pre-annealed large-grained samples using typical and optimized conditions clearly showed a sharpening of the depth profile in the latter case,<sup>[52]</sup> thus demonstrating the dual benefits of depth profiling on large grained samples with optimized SIMS conditions.

## 4. Experimental Procedures

Tracer diffusion experiments were carried out on pure Mg specimens at various temperatures from 250 to  $475\ ^\circ\text{C}$ . Samples used in this study were transferred between ORNL (sample preparation, annealing), Virginia Tech (SIMS, polishing) and University of Central Florida (isotope deposition) using special containers that protected the samples from movement and minimized exposure to the environment. Pure Mg (99.95% weight) rods (7.9 mm outer diameter, 25 mm length) were obtained from Alfa Aesar. The impurity analysis (in ppm) that was provided for a typical lot of pure Mg rods used in this study is listed in Table 1. The small average grain size and the broad grain size distribution in the as-received Mg rod samples (Fig. 4a) was found to be unsuitable for accurate SIMS depth profiling (discussed in Section 3.4).<sup>[52]</sup> Additionally, in order to use the thin or thick-film solution for bulk diffusion, it was necessary to be in the initial part of the Harrison B regime,<sup>[26,32,37]</sup> which required an annealing treatment to increase the grain size. An annealing treatment on a test sample at  $545\ ^\circ\text{C}$  for 14.5 h in the modified Shewmon-Rhines capsule was able to accomplish this objective (Fig. 3), resulting in a grain size in excess of  $500\ \mu\text{m}$  and a preferred orientation that was close to  $(2\bar{1}10)$  when

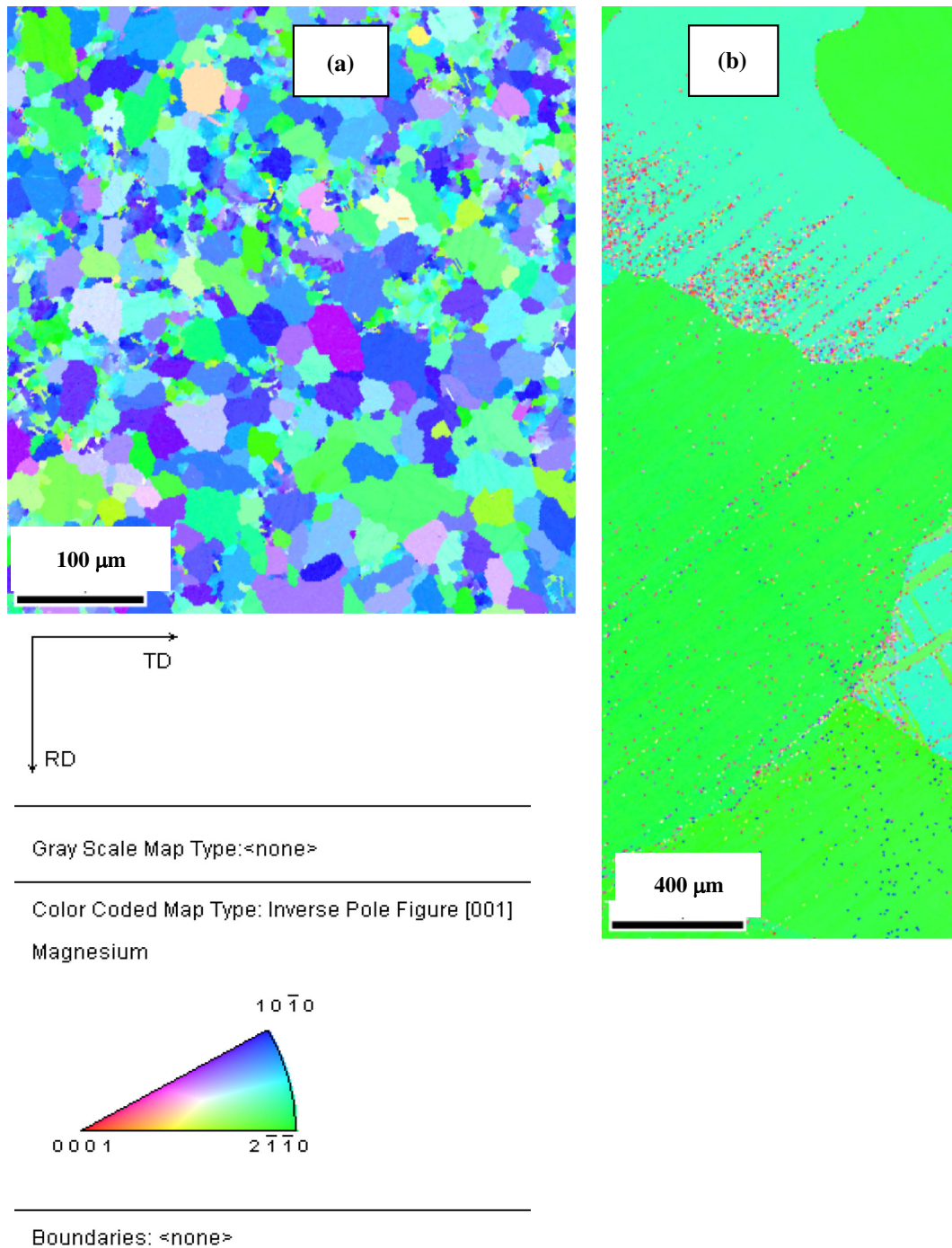


**Fig. 4** Electron Backscatter Diffraction (EBSD) map (inverse pole figure) of grain orientations in a cross-section of a pure polycrystalline Mg rod specimen: (a) as-received, (b) after an annealing treatment at 545 °C for 14.5 h

**Table 1** Composition specifications (in weight percent) of a typical pure Mg lot provided by Alfa Aesar

	Mg	Al	Cu	Mn	Ni	Si	Fe	Ca	Pb	Sn	Zn	Others (Total)
Lot 1	99.95	0.0030	0.0003	0.0028	0.0004	0.0030	0.0026	0.0010	0.0010	<0.0010	0.0040	0.03 max

imaged on the rod cross-section, which indicated that the measured tracer diffusivity along the rod (extrusion) axis would be in a direction approximately perpendicular ( $\perp$ ) to the c-axis of the hexagonal close packed (hcp) crystal, or parallel to the basal plane as argued by Shewmon and Rhines<sup>[44]</sup> (Fig. 4b). Samples that were sectioned in a direction parallel to the rod axis would have a tracer diffusion direction that was nearly parallel ( $\parallel$ ) to the c-axis of the hcp crystal. For the samples used in this study, the pre-annealing treatment was carried out at 595 °C for 9 h, which was considered to be reasonably similar to that at the lower temperature of 545 °C for 14.5 h.

Most of the Mg rods used in this study were cross-sectioned into smaller “normal” samples (~2-3 mm thick) using a diamond saw. A few samples were also sectioned in a direction parallel to the rod axis (orthogonal or “ortho” samples). Samples were hand polished (Buehler EcoMet 3000 polisher) in multiple steps starting with a rough polish (800 grit sandpaper with water for 30 s), medium polish with multiple diamond suspensions (9, 3 and 1  $\mu\text{m}$ ) and fine polish (0.3  $\mu\text{m}$  alumina suspension followed by 0.02  $\mu\text{m}$  colloidal silica). Thus the final surface finish was expected to be approximately 20 nm. While this polishing recipe utilized de-ionized (DI) water as the primary solvent medium, there are other polishing recipes for Mg that have utilized non-aqueous solvents throughout with reasonable success.

The polished Mg samples were then coated with a thin isotopic film of <sup>25</sup>Mg using the UHV sputter deposition system that was previously discussed (3.2). The conditions used for Mg isotopic deposition were: (a) RF pre-clean of the native oxide (126 W, 20 sccm Ar at 5 mTorr for 60 s); (b) Mg deposition at 50 W DC, 20 sccm Ar at 5 mTorr for 50 s. X-ray Photoelectron Spectroscopy (XPS) analysis confirmed the low (<5%) oxygen levels in the deposited Mg films. The thickness of the film within a circle of ~30 mm in diameter on the substrate was measured to be about 120  $\pm$  20 nm using a surface profilometer, with the higher thickness measured near the center. Approximately, 8 circular samples within a 30 mm diameter circle on the substrate could be coated uniformly with the specified thickness in a single deposition run. Precise knowledge of the coating thickness was not essential, since a non-linear fit of the SIMS depth profile data to the thin-film solution provided the thickness as a fitting parameter.

#### 4.1 Tracer Diffusion Annealing

The initial tracer-coated pure Mg samples (Set 1) were annealed at three nominal temperatures (300, 350 and 400 °C) using a first iteration of the modified Shewmon-Rhines annealing capsule that was enclosed in a sealed quartz capsule and inserted into a pre-heated copper block (Fig. 3). The nominal diffusion time at each nominal temperature (Table 2) was selected based on an approximate calculation of the total tracer diffusion penetration depth ( $\sim 6\sqrt{Dt}$ ), assuming a tracer diffusivity from previous Mg radiotracer data by Shewmon.<sup>[44]</sup> This enabled the selection of diffusion times that resulted in SIMS depth profile measurements that had a good dynamic signal range (one to

**Table 2 Nominal tracer diffusion annealing temperatures and times**

Nominal temperature		Nominal time	
°C	K	h	s
250	523	131	471,600
300	573	4	14,400
350	623	1	3,600
400	673	0.5	1,800
475	748	0.167	600

two orders) with sputtered depths that were usually less than 15  $\mu\text{m}$  (except for the 475 °C sample where the depth was ~23  $\mu\text{m}$ ). Since the initial version of the capsule did not have a thermocouple in the lid, the temperature-time profiles for this first set of samples were obtained using similar size control samples equipped with a thermocouple and subjected to the identical annealing conditions. From these profiles, corrections for the effective diffusion times, to account for start-up and cool-down times, were computed using a numerical integration method described by Rothman (p 21 of Ref 22):

$$t_{\text{effective}} = \exp\left[-\frac{Q}{R}\left(\frac{1}{T(t)} - \frac{1}{T_{\text{anneal}}}\right)\right] dt \quad (\text{Eq 14})$$

where  $T_{\text{anneal}}$  is the average temperature in the flat region of the temperature-time profile which is usually very close to the nominal temperature, and  $Q$  is the activation energy that was initially based on the known value for Mg self-diffusion obtained from higher temperature radiotracer data (134 kJ/mol)<sup>[44]</sup>, and then refined (127 kJ/mol) when the final lower temperature diffusivities from this study were obtained.

Subsequent Mg samples (Set 2) were tracer diffusion annealed at nominal temperatures of 250 and 475 °C and suitable annealing times (Table 2) using an improved version of the capsule that had a thermocouple in the cap, and hence permitted direct temperature-time profile measurements that were subsequently used to correct for start-up and cool-down times. The 475 °C sample was annealed in a further improvement of the capsule that had fins on its outer walls (Fig. 3a) to permit faster heat-up and cool-down times, and hence minimize the time correction required. All samples were quenched in liquid nitrogen on completion of the diffusion anneals. A temperature-time profile for a sample annealed at 475 °C is shown in Fig. 5. The temperatures that were used for computing the effective diffusion anneal times (Table 3) and the final tracer diffusivities from the SIMS depth profiles corresponded to the average steady-state temperatures recorded on the temperature-time profiles. These temperatures and effective times seen in Table 3 were close to but not identical to the nominal temperatures and times initially selected.

A correction of about 9% to the diffusion time was computed for the Mg sample that was annealed at 475 °C for ~10 min. (Fig. 5), assuming the time was only counted above a temperature of ~300 °C, since the cumulative time spent by the sample at temperatures lower than this (either

during heat-up or cool-down) was found to have a negligible contribution to the effective time spent by the sample at the annealing temperature. For other samples annealed at lower temperatures and much longer times, the corrections were usually lower but depended upon when the time counter was initiated and terminated. In any case, a computation of the time correction is not relevant to the current study, since the numerical integration procedure (Eq 14) from the measured temperature-time profiles directly provided the effective time at the annealing temperature. Supplemental MS Excel files containing these calculations based on the temperature-time plots for the samples annealed at 250 and 475 °C are provided.

#### 4.2 SIMS Measurements

Typical SIMS conditions used for conducting depth profile measurements corresponded to the optimized conditions previously discussed in section 3.4. These conditions corresponded to an  $O_2^+$  primary ion beam with an extraction

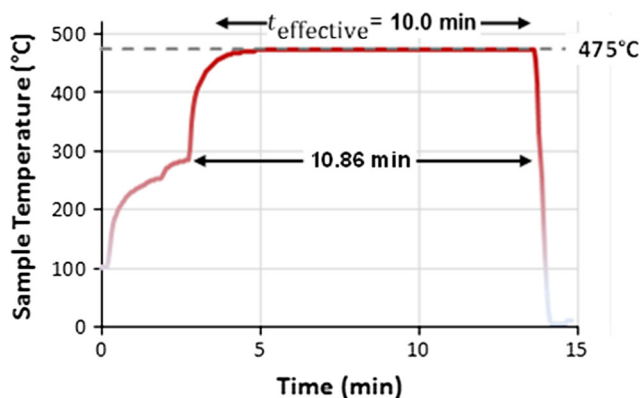


Fig. 5 Temperature-time profile for the Mg sample annealed at a temperature of  $\sim 475$  °C (748 K) and annealed for 10.86 min. The effective time computed using the numerical integration method described by Rothman [22] is 10 min

voltage of 5 kV, impact energy of 3 keV at an incidence angle of  $37.5^\circ$ , and an intentional O leak. Typical primary ion currents varied between 500-550 nA. The raster size was  $2000.1\text{cm}\mu\text{m} \times 2000.1\text{cm}\mu\text{m}$  but only the central area of  $33\ \mu\text{m}$  in diameter was used for extraction of the secondary  $Mg^+$  ions with the aid of an aperture lens system. The intensities for all the three Mg isotopes ( $^{24}, ^{25}, ^{26}Mg$ ) were measured as a function of time. From the calibrated sputter rate (typically a few nm/s) that was assumed to be constant during the analysis, the depth corresponding to the time at which the secondary ion signals were collected was determined. The sputter rate was calculated from the total measurement time and the final crater depth that was measured using a profilometer. As an example, the SIMS conditions used for the depth profiling for the  $349.8$  °C (623 K), annealed sample are provided in Table 4. For most of the samples in this study, depth profile measurements at two to four locations were typically done, see Table 5. Since the tracer diffusion annealing experiments for the “ortho” samples were done along with the “normal” samples in the same diffusion capsule, the temperatures and effective times reported are the same.

## 5. Results

A non-linear least square fit of the SIMS data using the Gaussian thin-film solution, Eq 9, was used to compute the tracer diffusion coefficients at the specified temperatures. A representative example of the fitted SIMS profile for the Mg tracer diffusion sample at  $349.8$  °C (623 K) for 0.919 h is shown in Fig. 6. The residual error is also shown in the figure. The non-linear fitting was done using the Solver in Microsoft Excel, which is available as an add-on feature. The supplemental files with this paper include the raw and analyzed SIMS data for the normal and ortho samples at the temperatures listed in Table 3. On account of surface artefacts in the near-surface region of SIMS depth profiles, the SIMS data from the first  $\mu\text{m}$  was not utilized for the non-

**Table 3 Measured tracer diffusion annealing temperatures and effective times computed after correcting for heat-up and cool-down times from the temperature-time profiles**

Temperature		EffectiveTime		Diffusion Direction	Comments
(°C)	(K)	(hrs)	(s)		
249.8	523	130.75	470,700	normal	Set 2
299.7	572.9	3.961	14,260	normal	Set 1
299.7	572.9	3.961	14,260	ortho	Set 1
349.8	623	0.919	3,308	normal	Set 1
349.8	623	0.919	3,308	ortho	Set 1
399.7	672.9	0.428	1,541	normal	Set 1
399.7	672.9	0.428	1,541	ortho	Set 1
474.7	747.9	0.166	598	normal	Set 2 (capsule with fins)

Normal: diffusion direction along rod axis; Ortho: diffusion direction perpendicular or orthogonal to rod axis. Set 1: Measurement of temperature-time profile on identical control sample (no tracer); Set 2: Direct measurement

**Table 4 SIMS conditions used for depth profiling the Mg sample annealed at 400 °C, 30 min**

Experimental conditions for X analysis				
Primary ions				O <sub>2</sub> <sup>+</sup>
Source extraction voltage				5 kV
Primary intensity				531 nA
Impact energy				3 keV
Incidence angle				37.5°
Beam blanking				No
Raster size				200 μm
Analyzed species(a)				
Elements	Det	Wt, s	Ct, s	Offset, V
24Mg	EM	0.72	1.04	0
25Mg	EM	0.72	1.04	0
26Mg	EM	0.72	1.04	0
Calibration parameters				
Sputter rate (Crater)				2.1653 nm/s
Mass spectrometer				
Vacuum in analysis chamber				3.070e−06 mbar
Polarity				+
Extraction voltage				1500 V
Max area				
Dynamic transfer optical system				Off
Electronic gate				71%
Contrast aperture				150 μm
Field aperture				400 μm
Analyzed area size				33 μm
Mass resolution (m/Δm) at 10%				3996
Energy band pass				15 eV
EM post-acceleration voltage				
Oxygen flooding				Yes
Liquid nitrogen trap, LN <sub>2</sub>				
Normal incidence electron gun				No

The SIMS system used was a Cameca IMS 7f-Geo at the Institute for Critical Technology and Applied Science—ICTAS, Virginia Tech  
(a) Total acquisition time: 4678.24 s, Reference signal: No, Interferences: –

linear fits. As previously mentioned, the non-linear fit also provides the tracer thickness and the background tracer concentration by using these as fitting parameters along with the diffusivity. The diffusivity was computed for each “spot” or location at which the SIMS data was collected, and then averaged. Table 5 provides the average Mg self-diffusion coefficients at various temperatures along with their standard deviations that were obtained from the present work. As a comparison, the diffusivities obtained from Shewmon’s radiotracer measurements in polycrystalline Mg rod specimens are also provided.<sup>[44]</sup>

Arrhenius fits for the normal and ortho tracer diffusivities obtained from the present study are shown in Fig. 7. The

fitted Arrhenius parameters are provided in Table 6. These are compared with the polycrystalline Arrhenius fits from the previous radiotracer measurements by Shewmon and Rhines.<sup>[44]</sup> Table 6 also provides the Arrhenius parameters for a fit that includes the polycrystalline data from both the present SIMS and radiotracer<sup>[44]</sup> studies (see Fig. 8).

## 6. Discussion

From Table 6, it is seen that the activation energy and pre-exponential factor for the present SIMS data for both the normal and ortho samples are lower than those obtained from the previous radiotracer studies by Shewmon and Rhines.<sup>[44]</sup> Thus the extrapolated Arrhenius fit of the high temperature radiotracer (normal samples) data to lower temperatures (<450 °C) where the SIMS measurements were carried out shows a negative deviation (Fig. 7). The measured SIMS self-diffusivity at 475 °C (748 K) compares quite favourably with that measured at 468 °C (741 K) using the radiotracer method, thus indicating that the two approaches are reasonably consistent with each other. This appears to be the case in spite of the differences in the annealing conditions employed (10 min—SIMS, 62 h—radiotracer), and the differences in the purity levels (99.95 wt.%—SIMS, ~99.9 wt.%—radiotracer<sup>[44]</sup>). An Arrhenius fit to the polycrystalline data from both types of measurements (Fig. 8) shows surprisingly good agreement over a broad range of temperatures, 250–627 °C (523–900 K), which is in line with the observation of Frank et al.,<sup>[37]</sup> who carried out Ni tracer diffusion studies in NiAl using a combination of radiotracer and SIMS measurements. This appears to suggest a single diffusion mechanism in pure Mg, although a more conclusive analysis would require single crystal diffusion measurements over a broad range of temperatures. For example, it can be noted that Shewmon’s high temperature data points<sup>[44]</sup> at 627 °C (900 K) suggest an upward curvature of the Arrhenius plot that is consistent with a small contribution from divacancies, see the review by Mundy.<sup>[54]</sup>

The self-diffusivities for the ortho samples were somewhat lower than the normal samples at 350 °C (623 K) and 400 °C (673 K), but were within the margin of error at 300 °C (573 K). The Arrhenius parameters for the ortho data were obtained over a very narrow temperature range of 300–400 °C. Extending the temperature range of measurements on such samples would be desirable for a better fit, and for exploring whether the differences in the self-diffusivities between the normal and ortho samples are significant.

The standard deviations in the diffusion data based on multiple SIMS profile measurements on individual samples at lower temperatures (250, 300 °C) were noticeably higher than those at higher temperatures. This may be indicative of a larger variation in the orientation-dependent diffusivity at lower temperatures, or a grain boundary diffusion field that affects SIMS profiles at locations that are less remote from grain boundaries. A one-to-one mapping of the SIMS diffusivities as a function of the local orientation and

**Table 5** Mg self-diffusion coefficients ( $D^*$ ) in polycrystalline rod specimens using SIMS (this work) and radiotracer techniques<sup>[44]</sup>

Temperature		$D^*(\text{m}^2/\text{s})$				Average $D^*$ ( $\text{m}^2/\text{s}$ )	s.d.	Diffusion Direction	Comments
°C	K	(1)	(2)	(3)	(4)				
474.7	747.9	$4.61 \times 10^{-14}$	$4.66 \times 10^{-14}$			$4.64 \times 10^{-14}$	0.8%	Normal	SIMS (this work)
399.7	672.9	$4.71 \times 10^{-15}$	$5.02 \times 10^{-15}$	$4.85 \times 10^{-15}$		$4.86 \times 10^{-15}$	3.2%	Normal	SIMS
349.8	623	$9.50 \times 10^{-16}$	$9.23 \times 10^{-16}$	$9.05 \times 10^{-16}$		$9.26 \times 10^{-16}$	2.4%	Normal	SIMS
299.7	572.9	$1.11 \times 10^{-16}$	$1.09 \times 10^{-16}$	$1.00 \times 10^{-16}$		$1.07 \times 10^{-16}$	5.5%	Normal	SIMS
249.8	523	$1.00 \times 10^{-17}$	$1.16 \times 10^{-17}$			$1.08 \times 10^{-17}$	10.5%	Normal	SIMS
399.7	672.9	$4.19 \times 10^{-15}$	$4.32 \times 10^{-15}$	$4.23 \times 10^{-15}$		$4.25 \times 10^{-15}$	1.6%	Ortho	SIMS
349.8	623	$7.47 \times 10^{-16}$	$7.71 \times 10^{-16}$	$8.63 \times 10^{-16}$		$7.94 \times 10^{-16}$	7.7%	Ortho	SIMS
299.7	572.9	$1.31 \times 10^{-16}$	$1.24 \times 10^{-16}$	$1.07 \times 10^{-16}$	$1.13 \times 10^{-16}$	$1.19 \times 10^{-16}$	9.3%	Ortho	SIMS
627	900.2	$2.06 \times 10^{-12}$	$2.10 \times 10^{-12}$			$2.08 \times 10^{-12}$	1.4%	Normal	Radiotracer
551	824.2	$3.60 \times 10^{-13}$				$3.60 \times 10^{-13}$	...	Normal	Radiotracer
468	741.2	$4.48 \times 10^{-14}$	$4.34 \times 10^{-14}$			$4.41 \times 10^{-14}$	2.2%	Normal	Radiotracer

The diffusion coefficients at a specified temperature were determined at two to four locations on a single specimen with the SIMS technique, while they were determined in 1-2 specimens with the radiotracer technique. Normal and ortho directions are the same definitions as in Table 3, s.d.: standard deviation

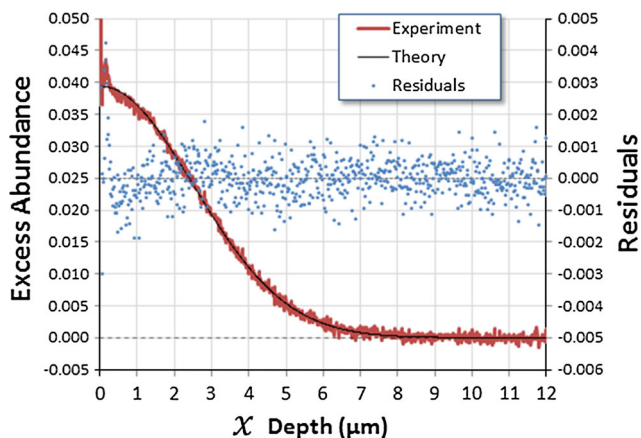


**Fig. 6** SIMS depth profile of the excess  $^{25}\text{Mg}$  tracer concentration (abundance) after tracer diffusion annealing at 349.8 °C (623 K) for 0.919 h. The non-linear fit using the Gaussian thin film solution and the residuals are also shown. Note that the data from the first micron of the measured depth profile was not used for the fit

position (relative to grain boundaries) at various temperatures would shed further light on this issue. It should be pointed out that the Cameca IMS 7f-Geo SIMS system utilized in this study does not have this capability. Hence a more laborious undertaking involving measurements on the same sample using independent instruments for SIMS and EBSD mapping would be needed for such studies. However, it is anticipated that future Focussed Ion Beam (FIB)—EBSD systems equipped with mass spectrometry capability (e.g., Time of Flight SIMS) may be extremely valuable in tracer diffusivity mapping as a function of orientation in polycrystalline matrices, especially those having a high degree of anisotropy.

The polycrystalline self-diffusivities in Mg measured using either the SIMS (this work) or radiotracer methods<sup>[44]</sup>

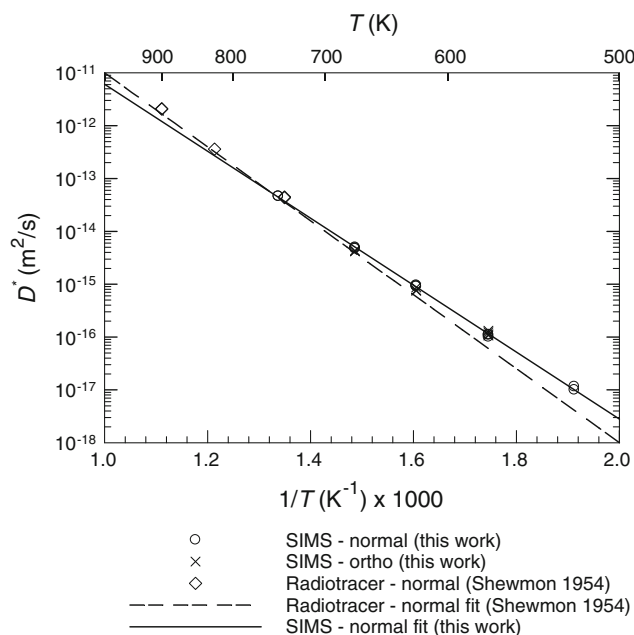


**Fig. 7** Self-diffusion data for polycrystalline Mg measured using SIMS (this work) and radiotracer (Shewmon and Rhines<sup>[44]</sup>) methods. The diffusion direction is along the rod axis for “normal” samples and perpendicular to the rod axis for “ortho” samples. The independent Arrhenius fits to the SIMS and radiotracer data for normal samples are also shown

were higher than the experimental single crystal diffusivities reported<sup>[19,45]</sup>, which in turn are higher than the theoretical predictions.<sup>[43]</sup> Thus it appears that in both methods, the effect of grain boundary diffusion cannot be completely ignored, even though the grain sizes were quite large in both cases (over 500  $\mu\text{m}$ ). A SIMS study as a function of grain size and grain orientation in isotropic and anisotropic materials at various temperatures would be helpful in

**Table 6 Arrhenius parameters for the Mg-self diffusion coefficients determined using the SIMS (this work) and radiotracer techniques<sup>[44]</sup>**

Measurement technique	$D_0, \text{m}^2\text{s}^{-1}$	$Q$		Temperature range	Comments
		(kJ/mol)	(kcal/mol)		
SIMS (this work)	$1.32 \times 10^{-5}$	121.3	29.0	250-475 °C (523-748 K)	Poly, normal, 99.95%
SIMS (this work)	$3.3 \times 10^{-6}$	114.6	27.4	300-400 °C (573-673 K)	Poly, ortho, 99.95%
Radiotracer <sup>[44]</sup>	$1.0 \times 10^{-4}$	133.9	32.1	468-627 °C (741-900 K)	Poly, normal, ~99.9%
Combined (SIMS + radiotracer <sup>[44]</sup> )	$3.33 \times 10^{-5}$	125.9	30.1	250-627 °C (523-900 K)	Poly, normal

The Arrhenius parameters for the combined data are also shown.  $D_0$  is the pre-exponential factor and  $Q$  is the activation energy; poly: polycrystalline; normal and ortho are defined in Table 3. Purity levels of Mg are provided in weight percent

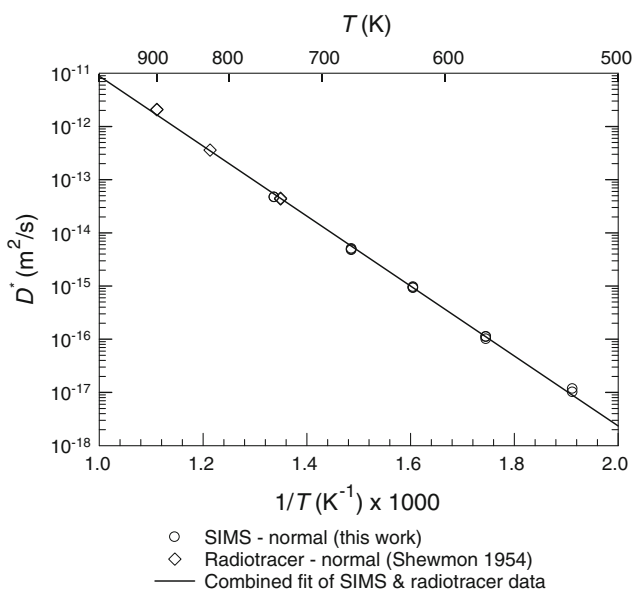


**Fig. 8** Arrhenius fit of Mg self-diffusion data using both SIMS (this work) and radiotracer data<sup>[44]</sup> in polycrystalline Mg (normal samples)

assessing the role of grain boundary diffusion and orientation-dependent diffusivity on bulk diffusivity measurements in the initial Harrison B region. Data from such measurements could then be compared with corresponding single crystal measurements using both SIMS and radiotracer methods.

Even though SIMS-based tracer diffusion studies are more convenient than radiotracer diffusion studies, there is still a need to develop more efficient procedures for gathering SIMS data in order to facilitate the development of tracer diffusion databases that permit the use of the complete Onsager diffusion formalism. One such method based on an interdiffusion, isotopic analysis in a diffusion couple was recently discussed by Belova et al.<sup>[55]</sup> Additional high-throughput methods involving diffusion couples or co-deposition methods for alloys may also be explored for such measurements.

Since some naturally occurring elements in the periodic table are monoisotopic (e.g., Al, Co, Mn, etc.), it is essential

to carry out radioactive tracer diffusion measurements in such cases using the conventional approach.<sup>[22]</sup> A dedicated SIMS system could also be employed for measurements involving radioactive isotopes, though such systems are not common. The recent availability of the rare and expensive  $^{26}\text{Al}$  radioactive isotope<sup>[48]</sup> would be a good test case for more efficient tracer diffusion measurements, noting that Al tracer diffusion data in many commercial Al-alloy systems are not easily available.

An extension of this study to SIMS-based tracer diffusion measurements in Mg alloys is expected in a future publication.

## 7. Conclusions

The SIMS-based stable isotopic technique was used to measure the bulk self-diffusion coefficient of Mg at various temperatures ranging from 250 to 475 °C (523 to 748 K) in large-grained polycrystalline specimens of high purity Mg. The diffusivity at the highest temperature of 475 °C (748 K) compared reasonably well with the radiotracer measurement of Shewmon and Rhines<sup>[44]</sup> at 468 °C (741 K). An Arrhenius fit that included both the SIMS and radiotracer bulk self-diffusion data in polycrystalline Mg rod specimens along a direction that was parallel to the rod axis gave good agreement with the measured diffusivities across a broad temperature range of 250-627 °C (523-900 K).

Special experimental techniques developed during the course of this work included a UHV deposition system for low-oxygen isotopic thin-film deposition, and a modified Shewmon-Rhines annealing capsule for accurate temperature-time profile measurements of Mg tracer diffusion samples in a protected environment. Optimum conditions for minimizing sputter-roughening during SIMS depth profiling were established and utilized for the tracer diffusion measurements. A numerical procedure was employed to correct for heat-up and cool-down time corrections from the temperature-time profiles. A least-squares method based on the Gaussian thin-film solution was successfully used to obtain the diffusion coefficients along with the background tracer concentrations and the initial tracer film thicknesses from the measured SIMS depth profiles.

## Acknowledgments

The authors are grateful for the support provided by the U.S. Department of Energy (DOE), Assistant Secretary for Energy Efficiency and Renewable Energy (EERE), Office of Vehicle Technologies as part of the Automotive Lightweight Materials Program under contract DE-AC05-00OR22725 with UT-Battelle, LLC. The authors thank the ORNL isotope processing facility, including Scott Aaron and Lee Zevenbergen for providing the enriched  $^{25}\text{Mg}$  isotopic foils used in this work and for helpful discussions. The technical expertise provided by Edward Kenik (EBSD analysis) and Harry Meyer (XPS analysis) at the High Temperature Materials Laboratory (HTML) is recognized. The authors acknowledge Edward Dein at the Advanced Materials Processing and Analysis Center (AMPAC) clean room facility, University of Central Florida (UCF) for his assistance with the UHV PVD system and the isotopic deposition experiments. The assistance of Jay Tuggle and the students of one of the authors, J. Hunter, at Virginia Tech during the course of this project are appreciated. The authors thank Sarah Brennan and the graduate students of one of the authors, Y. Sohn, and Mikhail Klimov (SIMS specialist) at UCF for their assistance during various stages of this work. The authors appreciate the many fruitful discussions related to SIMS with Peter Todd, formerly at ORNL and now at Nebulytics, Inc. in Oak Ridge. The authors thank John Allison, Robert McCune and the staff associated with the Mg-ICME initiative for their support and encouragement. The support of Carol Schutte, William Joost and Joe Carpenter with the DOE Vehicle Technologies Program, and Phil Sklad and David Warren at ORNL are gratefully acknowledged.

## References

1. A.R. Allnatt and A.B. Lidiard, *Atomic Transport in Solids*, Cambridge University Press, Cambridge, 1993
2. J. Philibert, *Atom Movements: Diffusion and Mass Transport in Solids*, Editions de Physique, Les Ulis, 1991
3. J.R. Manning, *Diffusion Kinetics for Atoms in Crystals*, Van Nostrand, Princeton, 1968
4. J.R. Manning, Correlation Factors for Diffusion in Nondilute Alloys, *Phys. Rev. B*, 1971, **4**, p 1111-1121
5. A.B. Lidiard, A Note on Manning's Relations for Concentrated Multicomponent Alloys, *Acta Metall.*, 1986, **34**, p 1487-1490
6. A.R. Allnatt, I.V. Belova, and G.E. Murch, Diffusion Kinetics in Dilute Binary Alloys with the H.C.P. Crystal Structure, *Phil. Mag.*, 2014, **94**, p 2487-2504
7. M. Koiwa and S. Ishioka, Random Walks and Correlation Factors in Diffusion via the Vacancy Mechanism in Hexagonal-Close-Packed Lattices, *Phil. Mag. A*, 1983, **47**, p 767-774
8. L.K. Moleko, A.R. Allnatt, and E.L. Allnatt, A Self-Consistent Theory of Matter Transport in a Random Lattice Gas and Some Simulation Results, *Phil. Mag. A*, 1989, **59**, p 141-160
9. J.S. Kirkaldy and D.J. Young, *Diffusion in the Condensed State*, Institute of Metals, London, 1987
10. I.V. Belova and G.E. Murch, Relations between Interdiffusivities and Intrinsic Diffusivities in Ternary and Quaternary Alloys, *Phil. Mag. Lett.*, 2003, **83**, p 73-77
11. L.S. Darken, Diffusion, Mobility and Their Interrelation Through Free Energy in Binary Metallic Systems, *Trans. AIME*, 1948, **175**, p 184-201
12. A. Borgenstam, A. Engström, L. Höglund, and J. Ågren, DICTRA, a Tool for Simulation of Diffusional Transformations in Alloys, *J Phase Equilib.*, 2000, **21**, p 269-280
13. J.O. Andersson, T. Helander, L. Höglund, P.F. Shi, and B. Sundman, Thermo-Calc and DICTRA, Computational Tools for Materials Science, *Calphad*, 2002, **26**, p 273-312
14. M.J.H. van Dal, M.C.L.P. Pleumeekers, A.A. Kodentsov, and F.J.J. van Loo, Diffusion Studies and Re-examination of the Kirkendall Effect in the Au-Ni System, *J Alloy Compd.*, 2000, **309**, p 132-140
15. N.S. Kulkarni, Ph.D. thesis, University of Florida, 2004, Appendix E
16. C.E. Campbell, W.J. Boettinger, and U.R. Kattner, Development of a Diffusion Mobility Database for Ni-Base Superalloys, *Acta Mater.*, 2002, **50**, p 775-792
17. J. Allison, D. Backman, and L. Christodoulou, Integrated Computational Materials Engineering: A New Paradigm for the Global Materials Profession, *JOM*, 2006, **58**, p 25-27
18. Materials Genome Initiative for Global Competitiveness, white paper, 2011. <http://www.whitehouse.gov/mgi>
19. P.G. Shewmon, Self-Diffusion in Magnesium Single Crystals, *JOM*, 1956, **206**, p 918-922
20. J.L. Routbert, S.J. Rothman, and J.N. Mundy, Oxygen Tracer Diffusion in  $\text{YBa}_2\text{Cu}_3\text{O}_8$ , *Phys. Rev. B*, 1993, **48**, p 7505-7512
21. I. Kaur, Y. Mishin, and W. Gust, *Fundamentals of Grain and Interface Boundary Diffusion*, Wiley, New York, 1995
22. S.J. Rothman, The Measurement of Tracer Diffusion Coefficients in Solids, *Diffusion in Crystalline Solids*, G.E. Murch and A.S. Nowick, Ed., Academic Press, Orlando, FL, 1984, p 1-61
23. J. Crank, *The Mathematics of Diffusion*, 2nd ed., Oxford University Press, Oxford, 1980
24. P. Shewmon, *Diffusion in Solids*, 2nd ed., The Minerals, Metals & Materials Society (TMS), Warrendale, PA, 1991
25. W. Petuskey, *Diffusion Analysis Using Secondary Ion Mass Spectroscopy (SIMS), Nontraditional Methods in Diffusion*, The Metallurgical Society of AIME, Philadelphia, 1983, p 179-203
26. R.A. De Souza and M. Martin, Probing Diffusion Kinetics with Secondary Ion Mass Spectrometry, *MRS Bull.*, 2009, **34**, p 907-914
27. A. Benninghoven, F.G. Rüdener, and H.W. Werner, *Secondary Ion Mass Spectrometry: Basic Concepts, Instrumental Aspects, Applications, and Trends*, Wiley, New York, 1987
28. J.L. Hunter, Jr., Chapter 6: Improving Depth Profile Measurements of Natural Materials: Lessons Learned from Electronic Materials Depth-Profiling, in *Secondary Ion Mass Spectrometry in the Earth Sciences: Gleaning the Big Picture from a Small Spot*, MAC Short Course Series, Vol. 41, M. Fayek, Ed., Mineralogical Association of Canada, Toronto, 2009, p 132-148
29. V. Randle and O. Engler, *Introduction to Texture Analysis*, CRC Press, Boca Raton, 2000
30. W. Gust, M.B. Hintz, A. Lodding, R. Lučić, H. Odelius, B. Predel, and U. Roll, Applicability of SIMS in the Study of Grain Boundary Diffusion, *J. Phys.*, 1995, **46**(C4), p 475-482
31. J. Goldstein, D.E. Newbury, D.C. Joy, C.E. Lyman, P. Echlin, L. Sawyer, and J.R. Michael, *Scanning Electron Microscopy and X-Ray Microanalysis*, 3rd ed., Springer, New York, 2007
32. L.G. Harrison, Influence of Dislocations on Diffusion Kinetics in Solids with Particular Reference to the Alkali Halides, *Trans Faraday Soc.*, 1961, **57**, p 1191-1199
33. C. Herzig and S.V. Divinski, Grain Boundary Diffusion in Metals: Recent Developments, *Mat. T. JIM*, 2003, **44**, p 14-27



34. F. Christien, C. Downing, K.L. Moore, and C.R.M. Grovenor, Quantitative Grain Boundary Analysis of Bulk Samples by SIMS, *Surf. Interface Anal.*, 2012, **45**, p 305-308
35. S. Swaroop, M. Kilo, C. Argirusis, G. Borhardt, and A.H. Chokshi, Lattice and Grain Boundary Diffusion of Cations in 3YTZ Analyzed using SIMS, *Acta Mater.*, 2005, **53**, p 4975-4985
36. T.F. Kelly, D.J. Larson, K. Thompson, R.L. Alvis, J.H. Bunton, J.D. Olson, and B.P. Gorman, Atom Probe Tomography of Electronic Materials, *Annu. Rev. Mater. Res.*, 2007, **37**, p 681-727
37. St Frank, S.V. Divinski, U. Södervall, and C. Herzig, Ni Tracer Diffusion in the B2-Compound NiAl: Influence of Temperature and Composition, *Acta Mater.*, 2001, **49**, p 1399-1411
38. A. Luo, Magnesium: Current and Potential Automotive Applications, *JOM*, 2002, **54**, p 42-48
39. S. Fujikawa, Diffusion in Magnesium, *Jpn. Inst. Light Met.*, 1992, **42**, p 822-825
40. J. Combronde and G. Brebec, Diffusion of Ag, Cd, In, Sn and Sb in Magnesium, *Acta Metall.*, 1972, **20**, p 37-44
41. K. Lal, Diffusion of Various Elements in Magnesium, CEA Report, 1967, R 3136, p 54
42. S. Brennan, A.P. Warren, K.R. Coffey, N. Kulkarni, P. Todd, M. Kilmov, and Y. Sohn, Aluminum Impurity Diffusion in Mg, *J. Phase Equilib.*, 2012, **33**, p 121-125
43. S. Ganeshan, L. Hector, Jr., and Z.-K. Liu, First-Principles Calculations of Impurity Diffusion Coefficients in Dilute Mg Alloys Using the 8-Frequency Model, *Acta Mater.*, 2011, **59**, p 3214-3228
44. P. Shewmon and F. Rhines, Rate of Self-Diffusion in Polycrystalline Magnesium, *Trans. AIME*, 1954, **250**, p 1021-1025
45. J. Combronde and G. Brebec, Anisotropy for Self-Diffusion in Magnesium, *Acta Metall.*, 1971, **19**, p 1393-1399
46. A.M. Brown and M.F. Ashby, Correlations for Diffusion Constants, *Acta Metall.*, 1980, **28**, p 1085-1101
47. J.N. Mundy, H.A. Hoff, J. Pelleg, S.J. Rothman, and L.J. Nowicki, Self-diffusion in Chromium, *Phys. Rev. B*, 1981, **24**, p 658-665
48. National Isotope Development Center, USDOE, Office of Science. <http://isotopes.gov/>
49. R.T. DeHoff, *Thermodynamics in Materials Science*, CRC/Taylor & Francis, Boca Raton, 2006
50. T. Kumar, A. Kumar, D.C. Agarwal, N. Prasad Lalla, and D. Kanjilal, Ion Beam-generated Surface Ripples: New Insight in the Underlying Mechanism, *Nanoscale Res. Lett.*, 2013, **8**, p 336
51. F.A. Stevie, J.L. Moore, S.M. Merchant, C.A. Bollinger, and E.A. Dein, Secondary Ion Mass Spectrometry Analysis of a Three-Level Metal Structure Using Sample Rotation, *J. Vac. Sci. Technol. A*, 1994, **12**, p 2363-2367
52. J. Tuggle, A. Giordani, N. Kulkarni, R. Warmack, and J. Hunter, Secondary ion mass spectrometry for Mg tracer diffusion: issues and solutions, *Surf. Interface Anal.*, 2014. doi:10.1002/sia.5618
53. J.F. Ziegler, The Stopping and Range of Ions in Matter (SRIM), 2013 software, <http://www.srim.org/>
54. J.N. Mundy, Diffusion in Solids: Unsolved Problems, Chapter 1, *Defect and Diffusion Forum*, Vol. 83, G.E. Murch, Ed., TTP, Zürich, 1992, p 1-18
55. I.V. Belova, N.S. Kulkarni, Y.H. Sohn, and G.E. Murch, Simultaneous Measurement of Tracer and Interdiffusion Coefficients: An Isotopic Phenomenological Diffusion Formalism for the Binary Alloy, *Phil. Mag.*, 2013, **93**, p 3515-3526